



Research article

Multi-objective optimization of a photovoltaic thermal-compound sensible rotary heat exchanger system using exergo-economic and enviro-economic approaches

Wei He^a, Azeez A. Barzinjy^{b,c}, S. Khanmohammadi^d, Amin Shahsavari^d, M.A. Moghimi^e, Masoud Afrand^{f,g,**}

^a School of Economics and Management, Minjiang University, Fuzhou, 350108, China

^b Department of Physics, College of Education, Salahaddin University-Erbil, Kurdistan Region, Iraq

^c Department of Physics Education, Faculty of Education, Tishk International University, Erbil, Kurdistan Region, Iraq

^d Department of Mechanical Engineering, Kermanshah University of Technology, Kermanshah, Iran

^e Department of Mechanical and Aeronautical Engineering, University of Pretoria, Pretoria, South Africa

^f Laboratory of Magnetism and Magnetic Materials, Advanced Institute of Materials Science, Ton Duc Thang University, Ho Chi Minh City, Viet Nam

^g Faculty of Applied Sciences, Ton Duc Thang University, Ho Chi Minh City, Viet Nam



ARTICLE INFO

Keywords:

Building integrated photovoltaic thermal (BIPVT)
Sensible rotary heat exchanger (SRHX)
Multi-objective genetic algorithm optimization
Exergo-economic
Enviro-economic

ABSTRACT

This paper presents exergo-economic and enviro-economic assessment of a novel building integrated photovoltaic thermal-compound sensible rotary heat exchanger (BIPVT-SRHX) system. The innovative BIPVT-SRHX system preheats/precools the outdoor air in winter/summer and generates electric power. The performance of the system are analyzed from the energy/exergy viewpoints for Kermanshah, Iran climatic conditions. Then, the multi-objective genetic algorithm (MOGA) optimization is used to determine the optimum values of geometric and operating parameters in order to maximize the annual average exergo-economic and enviro-economic aspects of the system. The considered geometric and operating parameters include the length, width and depth of the air channel located underneath the PV modules, the air mass flow rate, and the diameter, rotational velocity and length of the SRHX. Moreover, the annual performance of the optimized and non-optimized BIPVT-SRHX systems are compared. The results showed that the annual average exergo-economic and enviro-economic aspects of the optimized BIPVT-SRHX system are 0.0076 \$/annum and 246.9 kWh/\$, respectively. Furthermore, it was found that the annual average enviro-economic aspect, annual average exergo-economic aspect, and yearly sum of CO₂ mitigation of the optimized BIPVT-SRHX system are respectively 36.8%, 23.1% and 37.7% higher than the non-optimized system.

1. Introduction

Solar or photovoltaic cells directly convert sunlight to electricity. The process of electricity generation in solar cells is eco-friendly (clean and noiseless) and competitive with fossil-based sources. Therefore, the temptations of using PV modules are constantly increased. Measurements have shown that boosting the temperature of the PV panels causes a reduction in their open circuit voltage and, consequently, to decline their efficiency. Therefore, it is essential to reduce the temperature of the PV panels. This can be achieved by pumping a fluid under or above

the panels. Systems that use this method are called the PVT system.

In recent years, the BIPVT systems have attracted substantial attention from researchers. Chen et al. (2017) presented the modeling and optimization of a heat pipe PVT heat pump system. In the proposed system, the removed heat from PVT collectors was utilized in a heat pump. To achieve the best system performance, the capacity of the heat pump and the number of collectors were optimized. Modjinou et al. (2017) assessed the performance of a novel micro-channel heat pipe PVT collector. They found that the highest instantaneous thermal and electrical efficiencies are 54% and 7.6%, respectively. Di Capua et al. (Di Capua et al., 2018) used a numerical approach to evaluate the

** Corresponding author. Laboratory of Magnetism and Magnetic Materials, Advanced Institute of Materials Science, Ton Duc Thang University, Ho Chi Minh City, Viet Nam.

E-mail addresses: hewei.mju@gmail.com (W. He), azeez.azeez@su.edu.krd (A.A. Barzinjy), a.shahsavari@kut.ac.ir (A. Shahsavari), masoud.afrand@tdtu.edu.vn (M. Afrand).

<https://doi.org/10.1016/j.jenvman.2019.109767>

Received 10 April 2019; Received in revised form 17 October 2019; Accepted 21 October 2019

Available online 5 November 2019

0301-4797/© 2019 Elsevier Ltd. All rights reserved.

Nomenclature	
C_c	heat capacity rate of cold air ($W K^{-1}$)
C_h	heat capacity rate of warm air ($W K^{-1}$)
C_{min}	minimum heat capacity rate ($W K^{-1}$)
c_p	specific heat capacity of air ($J kg^{-1} K^{-1}$)
$c_{p,c}$	specific heat capacity of cold air ($J kg^{-1} K^{-1}$)
$c_{p,h}$	specific heat capacity of warm air ($J kg^{-1} K^{-1}$)
$\dot{E}_{fan,BIPV/T}$	electricity demand of BIPVT fan (kWh)
$\dot{E}_{fan,c}$	electricity demand of cold air fan (kWh)
$\dot{E}_{fan,h}$	electricity demand of warm air fan (kWh)
$\dot{E}_{u,BIPV/T-cooling}$	useful power captured by BIPVT system during cooling mode (kWh)
$\dot{E}_{u,BIPV/T-heating}$	useful power captured by BIPVT system during heating mode (kWh)
$\dot{E}_{u,cooling}$	useful power captured by hybrid system during cooling mode (kWh)
$\dot{E}_{u,heating}$	useful power captured by hybrid system during heating mode (kWh)
$\dot{E}_{u,TW-cooling}$	useful power captured by TW system during cooling mode (kWh)
$\dot{E}_{u,TW-heating}$	useful power captured by TW system during heating mode (kWh)
h_c	convective heat exchange coefficient ($W K^{-1} m^{-2}$)
$h_{r,pv-b}$	radiative heat exchange coefficient between PV panels and back wall ($W K^{-1} m^{-2}$)
$h_{r,pv-s}$	radiative heat transfer coefficient between PV panels and sky ($W K^{-1} m^{-2}$)
h_w	wind convective heat exchange coefficient ($W K^{-1} m^{-2}$)
i	inflation rate
I_r	solar radiation intensity ($W m^{-2}$)
L	PV channel length (m)
\dot{m}_f	air mass current ($kg s^{-1}$)
$\dot{m}_{f,c}$	mass current of cold air ($kg s^{-1}$)
$\dot{m}_{f,h}$	mass current of warm air ($kg s^{-1}$)
P_s	net present cost (\$)
ΔP	pressure loss (Pa)
R_{en}	enviroeconomic parameter (\$/annum)
R_{ex}	exergoeconomic parameter (kWh/\$)
S	PV channel depth (m)
S_s	salvage value (\$)
T_a	ambient temperature (K)
T_b	back wall temperature (K)
$T_{c,i}$	entering temperature of cold air (K)
$T_{c,o}$	leaving temperature of cold air (K)
T_f	air temperature (K)
$T_{h,i}$	entering temperature of hot air (K)
$T_{h,o}$	leaving temperature of hot air (K)
T_{in}	entering temperature of air inside PV channel (K)
T_{mf}	mean air temperature inside PV channel (K)
T_{pv}	PV panel temperature (K)
U_b	bottom heat loss coefficient ($W K^{-1} m^{-2}$)
W	PV channel width (m)
$\dot{X}_{air,in}$	exergy of entering air (kWh)
$\dot{X}_{air,out}$	exergy of leaving air (kWh)
$\dot{X}_{c,i}$	exergy of entering cold air (kWh)
$\dot{X}_{c,o}$	exergy of leaving cold air (kWh)
$\dot{X}_{dest,BIPV/T}$	exergy loss inside the BIPVT system (kWh)
$\dot{X}_{dest,TW}$	exergy loss inside the TW system (kWh)
$\dot{X}_{el,PV}$	electrical exergy generated by PV panels (kWh)
$\dot{X}_{fan,c}$	electrical exergy demand of cold air fan (kWh)
$\dot{X}_{fan,h}$	electrical exergy demand of warm air fan (kWh)
$\dot{X}_{h,i}$	exergy of entering warm air (kWh)
$\dot{X}_{h,o}$	exergy of leaving warm air (kWh)
\dot{X}_{solar}	exergy of solar radiation (kWh)
$\dot{X}_{u,BIPV/T-cooling}$	useful exergy of the BIPVT system during cooling mode (kWh)
$\dot{X}_{u,BIPV/T-heating}$	useful exergy of the BIPVT system during heating mode (kWh)
$\dot{X}_{u,TW-cooling}$	useful exergy of the TW during cooling mode (kWh)
$\dot{X}_{u,TW-heating}$	useful exergy of the TW during heating mode (kWh)
z_{CO_2}	international carbon price (14.5 \$ per ton of CO_2)
Greek symbols	
α_{pv}	absorptance of PV panels
ε	wheel effectiveness
η_{el}	electrical conversion efficiency of PV panels (%)
η_{fan}	fan efficiency
ρ	air density ($kg m^{-3}$)
ϕ_{CO_2}	amount of CO_2 mitigation per annum (ton of CO_2 /annum)

performance of a high concentration PVT system integrated with a micro-channel heat sink (MCHS) with installed aligned and offset forward triangular ribs on the microchannel walls. The results showed that the aligned and offset rib distributions on the MCHS boosts the heat transfer 1.8 and 1.6 folds, respectively. Xia et al. (2018) developed and examined a model-based optimal control strategy for a PVT assisted ground source heat pump (GSHP-PVT) system. They utilized the simplified adaptive models and a genetic algorithm to recognize energy efficient control setting for GSHP-PVT system. It was observed that the optimal control strategy in comparison with a conventional control strategy can reduce energy use and intensify electricity production. Mousavi et al. (2018) numerically and experimentally analyzed the impact of copper foams filled with phase change materials (PCMs) on the energy matrices of a PVT collector. They found that the thermal output of the PVT system boosts by using copper foam filled with the PCM. Nahar et al. (2019) numerically evaluated the impacts of Reynolds number, Prandtl number, irradiation level and depth of flow channel on the thermal output of PVT systems. The findings revealed that the thermal efficiency boosts with augmenting the Reynolds number,

Prandtl number, and irradiation level while reduces by augmenting the channel depth.

One of the promising applications of the PVT systems is BIPVT system. Recently, some researchers have focused on design and performance evaluation of BIPVT assisted air conditioning systems. Shahsavari et al. (2011) suggested a BIPVT collector for cooling PV modules by outdoor/exhaust air in cooling/heating modes and generating electricity. It was shown that the suggested system has a considerable energy-saving potential. Additionally, the same group examined the energetic and exergetic optimization of the suggested collector (Khaki et al., 2017, 2018). Calise et al. (2017) evaluated the energy matrices of an innovative air conditioning system including concentrated PVT collectors (CPVT), fuel cell, electrolyzer and absorption chiller. The proposed system was capable of generating electricity as well as producing hot and cold air, domestic hot water, hydrogen and oxygen. They utilized TRNSYS software to examine the daily, weekly and yearly performance of the system. Additionally, an optimization and a sensitivity analysis were conducted to improve the system performance. The findings revealed that the total energy efficiency of the optimized PVT

system can reach above 80%. Yu et al. (2018) suggested an innovative solar gradient utilization system for combined photocatalytic oxidation technology and PVT system. The photocatalytic system utilized ultraviolet wavelength range of the impinging solar rays to drive photocatalytic degradation of indoor pollutants, and the PVT system absorbed visible and infrared wavelength ranges to produce electricity, warm air and hot water. The results indicated that the electrical efficiency of the system is about 0.174 considering both the generated electricity by PV modules and the saving electricity by purifying air. Liu et al. (2018) established a dynamic model for a PVT assisted thermoelectric ventilator system. In the proposed system, the PVT system produced electricity in winter and preheated the outdoor air. The preheated air was further heated using a thermoelectric ventilator. It was shown that the performance of the system improves by increasing the fresh air mass current. Shahsavari et al. (2018) investigated the feasibility of integrating a BIPVT collector with a SRHX. The proposed system contributed to a decrease in heating/cooling load of a building. The examined hybrid collector showed superior heat recovery performance in comparison with the BIPVT and SRHX systems. In another study (Khanmohammadi and Shahsavari, 2018), the same group optimized the performance of the BIPVT-SRHX system from the first law of thermodynamic perspective. It was found that the implementation of the proposed system could save respectively 217.3 kWh and 43871.5 kWh thermal and electrical energy in a year.

Exergy analysis is a practical technique to assess the productivity, efficiency, and sustainability of energy conversion systems. This is because of the fact that the exergetic performance of energy conversion systems strongly depends on its economic/environmental and sustainability aspects. Therefore, a more realistic analysis of the energy systems is possible only if the economic and environmental aspects of the system are included in the analysis. Improved exergy-based methodologies such as exergo-economic and enviro-economic approaches could be utilized to intensify the efficiency of energy systems in eco-friendly and a cost-effective way. Generally, exergo-economic and enviro-economic methods combine the exergy analysis with environmental and economic features, correspondingly, to obtain distinguished intuitive which is not achievable from the conventional exergy analysis. So the attention of many scholars has been drawn to the use of these techniques. Despite this fact, the literature review shows that the exergo-economic and enviro-economic performance of BIPVT collectors are rarely investigated. Singh and Tiwari (2017) compared the exergo-economic and enviro-economic features of single and double slope PVT solar distillation systems for same basin area under similar climatic conditions. It was depicted that the double slope system has superior exergo-economic and enviro-economic features. Tripathi et al. (2017) compared the exergo-economic aspect of three different series connected CPVT systems including non-covered, partially covered and fully covered N-CPVT collectors. As concluded, the non-covered collectors have the maximum exergo-economic aspect, 0.25 \$/kWh for 30 years of life time of the system. Sharaf et al. (Sharaf and Orhan, 2018) reported the exergo-economic assessment of two densely-packed CPVT systems consisting of parabolic dish concentrators, multi-junction PV (MJPV) cells, segmented thermoelectric generator (STEG) couples with interconnectors, and finned minichannel heat extractors (MHXs). In the first system, the receiver assembly components were connected thermally in-series, while they were connected thermally in-parallel in the second system. It was found that the thermally in-parallel configuration has a slight exergo-economic advantage. Shahsavari and Rajabi (2018) carried out the exergo-economic and enviro-economic analyses of a BIPVT system for Kermanshah, Iran climatic condition with considering the effects of the length, depth, and width of the duct below the PV and the inlet mass current on the proposed system. It was demonstrated that the exergo-economic aspect reduces by augmenting the flow rate, while it boosts with augmenting the duct length, duct depth, and duct width. Moreover, it was revealed that augmenting the flow rate, duct length and duct width leads to strengthen of the enviro-economic aspect, while

it is weakened with the increase of duct depth.

To the best of authors' knowledge, there is no previously published work presenting the exergo-economic and enviro-economic performances of hybrid BIPVT-SRHX systems. The goal of this work is to numerically evaluate the performance of a waste heat recovery system including a BIPVT collector and a SRHX for Kermanshah, Iran climatic conditions from both exergo-economic and enviro-economic viewpoints. In the proposed system, the outdoor air is preheated/precooled by recovering heat/cold from exhaust air in winter/summer. In addition, the system produces electric power, where a portion is consumed for system requirements and the rest can supply a part of building electricity demand. This numerical assessment is performed by utilizing MATLAB software.

2. System layout

The schematic configuration of the proposed BIPVT-SRHX system is illustrated in Fig. 1. This system operates in two different modes, namely cooling and heating modes. In the heating mode, the cold outdoor air enters a SRHX where preheated by absorbing heat from exhaust air. The preheated air is then sent inside the duct located under the PV panels. This induction has a dual impact on the system performance. Firstly, the PV modules are cooled and their efficiencies are increased. Secondly, the air temperature rises again by absorbing extra heat from the PV modules. In the cooling mode, the warm outdoor air enters a SRHX, gives off its heat to the exhaust air and, thus, is precooled. Also, following its exit from the SRHX, the exhaust air enters the PVT system, cools the PV modules and improves their electrical performances.

3. Energy analysis

3.1. BIPVT system

The schematic sketch of the suggested BIPVT system is demonstrated in Fig. 2. As displayed, L is the duct length, W is the duct width, and S is the duct depth. It is assumed that PV panels are of polycrystalline silicon type, SRHX is made of stainless steel, and heat transfer takes place under steady, one-dimensional conditions with uniform temperature of PV modules and back insulation wall at any instantaneous.

By solving the energy balance equations for different parts of the BIPVT system along with the boundary condition (i.e. $T_f|_{x=0} = T_{in}$), the air temperature at the distance x from the duct inlet is:

$$T_f(x) = \left(T_{in} - \frac{A_2}{A_1} \right) e^{-A_1 x} + \frac{A_2}{A_1} \quad (1)$$

where

$$A_1 = \frac{h_c W}{\dot{m}_f c_p} (2 - A_{1-1} - A_{1-2}) \quad (2a)$$

$$A_{1-1} = \frac{(h_c + (h_{r,pv-b} h_c / h_{r,pv-b} + U_b + h_c)) / (h_w + h_{r,g-s} + h_c + h_{r,pv-b})}{1 - (h_{r,pv-b}^2 / ((h_w + h_{r,g-s} + h_c + h_{r,pv-b})(h_{r,pv-b} + U_b + h_c))} \quad (2b)$$

$$A_{1-2} = \frac{\frac{h_{r,pv-b} ((h_c + (h_{r,pv-b} h_c / (h_{r,pv-b} + U_b + h_c))) / (h_w + h_{r,g-s} + h_c + h_{r,pv-b}))}{1 - (h_{r,pv-b}^2 / ((h_w + h_{r,g-s} + h_c + h_{r,pv-b})(h_{r,pv-b} + U_b + h_c))}}{h_{r,pv-b} + U_b + h_c} \quad (2c)$$

and

$$A_2 = \frac{h_c W}{\dot{m}_f c_p} (A_{2-1} + A_{2-2}) \quad (3a)$$

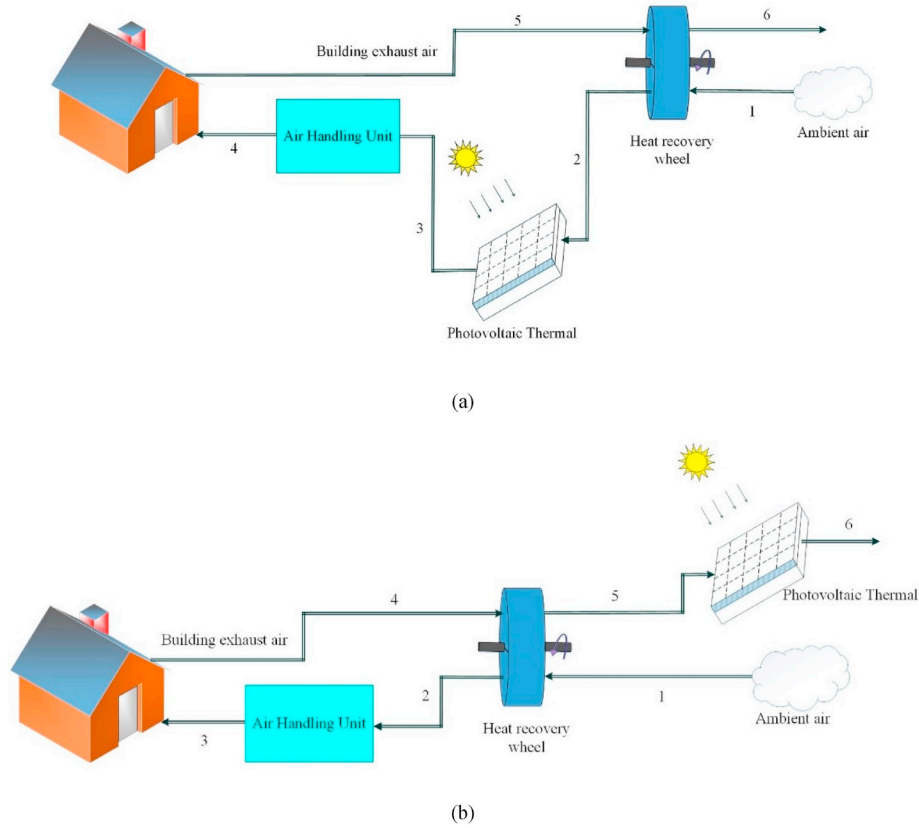


Fig. 1. Schematic diagram of the proposed BIPVT-SRHX system: (a) heating mode and (b) cooling mode.

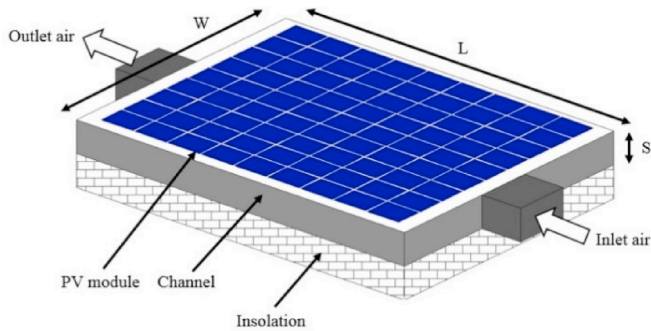


Fig. 2. Schematic of the studied BIPVT system (Shahsavari and Rajabi, 2018).

$$A_{2-1} = \frac{\alpha_{pv}(1 - \eta_{el})I_r + (h_w + h_{r,pv-s})T_a + \frac{h_{r,pv-b}U_bT_a}{h_w + h_{r,pv-s} + h_c + h_{r,pv-b}}}{1 - \left(h_{r,pv-b}^2 / (h_w + h_{r,g-s} + h_c + h_{r,pv-b}) (h_{r,pv-b} + U_b + h_c) \right)} \quad (3b)$$

$$A_{2-2} = \frac{\frac{\alpha_{pv}(1 - \eta_{el})I_r + (h_w + h_{r,g-s})T_a + \frac{h_{r,pv-b}U_bT_a}{h_w + h_{r,pv-s} + h_c + h_{r,pv-b}}}{h_{r,pv-b} + U_b + h_c}}{1 - \left(h_{r,pv-b}^2 / (h_w + h_{r,g-s} + h_c + h_{r,pv-b}) (h_{r,pv-b} + U_b + h_c) \right)} \quad (3c)$$

Consequently, the exit air temperature is:

$$T_L(x) = \left(T_{in} - \frac{A_2}{A_1} \right) e^{-A_1 L} + \frac{A_2}{A_1} \quad (4)$$

The mean temperature of the air is:

$$T_{mf} = \frac{1}{L} \int_0^L T_f(x) dx = \left(T_{in} - \frac{A_2}{A_1} \right) \frac{1}{A_1} (1 - e^{-A_1 L}) + \frac{A_2}{A_1} \quad (5)$$

The temperature of the PV modules and back insulation wall are:

$$T_{pv} = A_{2-1} + A_{1-1} T_{mf} \quad (6)$$

$$T_b = A_{2-2} + A_{1-2} T_{mf} \quad (7)$$

For in detail discussion of the computational procedure, please consult with Shahsavari et al. (Shahsavari et al., 2018; Khanmohammadi and Shahsavari, 2018).

3.2. SRHX system

The sensible wheel known as SRHX is a rotary air-to-air heat exchanger consists of a circular honeycomb matrix of heat-absorbing material, which is slowly rotated within two air streams. Rotation of the wheel allows the heat to be transferred to the cooler air as it passes through the wheel.

The schematic layout of the considered SRHX is shown in Fig. 3. The performance of the SRHX is assessed through the effectiveness-number of transfer units ($\epsilon - NTU$) technique. For sake of brevity, please consult with Shahsavari et al. (Shahsavari et al., 2018; Khanmohammadi and Shahsavari, 2018) for detail discussion of the method.

The exit temperature of the hot and cold streams of the SRHX can be obtained as follows:

$$T_{h,o} = T_{h,i} - \epsilon \frac{C_{min}(T_{h,i} - T_{c,i})}{C_h} \quad (8)$$

$$T_{c,o} = T_{c,i} + \epsilon \frac{C_{min}(T_{h,i} - T_{c,i})}{C_c} \quad (9)$$

Here $T_{c,i}$ is the entering temperature of cold air, $T_{h,i}$ is the entering temperature of hot stream, C_c is the heat capacity of cold air ($= \dot{m}_{f,c} c_{p,c}$ where $\dot{m}_{f,c}$ and $c_{p,c}$ are the mass current and specific heat of cold air stream, respectively), C_h is the heat capacity of hot stream ($= \dot{m}_{f,h} c_{p,h}$

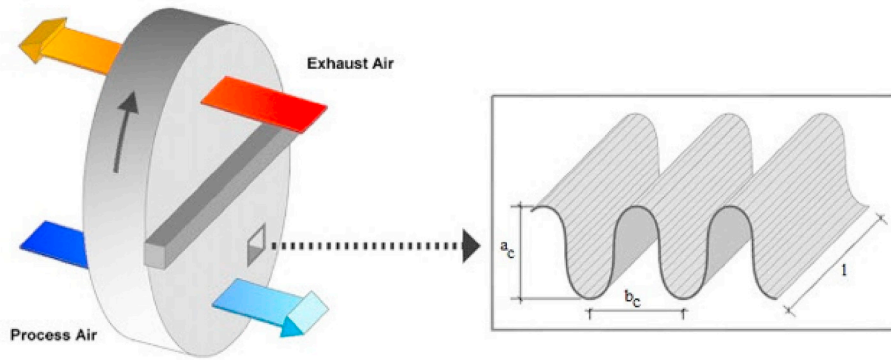


Fig. 3. Schematic layout of the considered SRHX system.

where $\dot{m}_{f,h}$ and $c_{p,h}$ are the mass current and specific heat of hot air stream, respectively), C_{min} is the minimum heat capacity rate ($= \min[C_c, C_h]$), and ε is the effectiveness of SRHX.

4. Exergy analysis

In thermodynamics, exergy is the potential of a system to cause a change as it achieves equilibrium with its environment. Despite energy, exergy can be consumed or destroyed, due to irreversibilities in any real process. Exergy assessment is performed based on the second law of thermodynamics.

Under steady-state operation, exergy balance of the SRHX dictates that the rate of exergy input must be equal to the rate of exergy output; yielding (Shahsavari and Khanmohammadi, 2019):

$$\dot{X}_{c,i} + \dot{X}_{h,i} + \dot{X}_{fan,c} + \dot{X}_{fan,h} = \dot{X}_{c,o} + \dot{X}_{h,o} + \dot{X}_{dest,TW} \quad (10)$$

where $\dot{X}_{c,i}$ is the exergy of cold air entering the SRHX, $\dot{X}_{h,i}$ is the exergy of hot air entering the SRHX, $\dot{X}_{c,o}$ is the exergy of cold air leaving the SRHX, and $\dot{X}_{h,o}$ is the exergy of hot air leaving the SRHX. Additionally, $\dot{X}_{fan,c}$ and $\dot{X}_{fan,h}$ are the exergy of electricity consumed by fans to blow cold and hot air streams inside the SRHX, respectively. Also, $\dot{X}_{dest,TW}$ in Eq. (10) denotes the exergy destructed through the SRHX.

The exergy of air streams are computed using the following equations (Khaki et al., 2017):

$$\dot{X}_{c,i} = \dot{m}_f c_p \left[T_{c,i} - T_a - T_a \ln \left(\frac{T_{c,i}}{T_a} \right) \right] \quad (11)$$

$$\dot{X}_{h,i} = \dot{m}_f c_p \left[T_{h,i} - T_a - T_a \ln \left(\frac{T_{h,i}}{T_a} \right) \right] \quad (12)$$

$$\dot{X}_{c,o} = \dot{m}_f c_p \left[T_{c,o} - T_a - T_a \ln \left(\frac{T_{c,o}}{T_a} \right) \right] \quad (13)$$

$$\dot{X}_{h,o} = \dot{m}_f c_p \left[T_{h,o} - T_a - T_a \ln \left(\frac{T_{h,o}}{T_a} \right) \right] \quad (14)$$

where T_a is the outdoor air temperature.

The exergy analysis of the BIPVT collector can be written as (Khaki et al., 2017):

$$\dot{X}_{air,in} + \dot{X}_{solar} + \dot{X}_{fan,BIPVT} = \dot{X}_{air,out} + \dot{X}_{el,PV} + \dot{X}_{dest,BIPVT} \quad (15)$$

where $\dot{X}_{air,in}$ is the exergy of air entering the BIPVT system, $\dot{X}_{air,out}$ is the exergy of air leaving the BIPVT system, and \dot{X}_{solar} is the solar radiation exergy, respectively. Also, $\dot{X}_{fan,BIPVT}$ is the exergy of electricity consumed by fan to blow air stream inside the BIPVT system and $\dot{X}_{el,PV}$ is the exergy of electricity generated by PV modules. Also, $\dot{X}_{dest,BIPVT}$ in Eq. (15) is the exergy destructed through the BIPVT system.

5. Estimation of performance metrics

The available energy of the BIPVT-SRHX system during the heating mode is calculated as:

$$\dot{E}_{u,heating} = \dot{E}_{u,TW-heating} + \dot{E}_{u,BIPVT-heating} \quad (16)$$

where

$$\dot{E}_{u,TW-heating} = \dot{m}_f c_p (T_{c,o} - T_{c,i}) - \left(\frac{\dot{E}_{fan,c} + \dot{E}_{fan,h}}{0.36} \right) \quad (17)$$

$$\dot{E}_{u,BIPVT-heating} = \dot{m}_f c_p [T_f(L) - T_{c,o}] + \left(\frac{\dot{E}_{el,PV} - \dot{E}_{fan,BIPVT}}{0.36} \right) \quad (18)$$

where $\dot{E}_{u,TW-heating}$ and $\dot{E}_{u,BIPVT-heating}$ are respectively the available energy of the SRHX and BIPVT systems during the heating mode, $\dot{E}_{fan,c}$ and $\dot{E}_{fan,h}$ are respectively the electric power consumed by fans to circulate cold and hot air streams inside the SRHX. In addition, $\dot{E}_{fan,BIPVT}$ is the electricity consumed by fan to circulate air through the BIPVT system and $\dot{E}_{el,PV}$ is the electric power generated by the PV modules. In the above formulas, the coefficient 0.36 is the conversion factor of the thermal power plant, which is used to convert high value electrical energy to low value thermal energy (Shahsavari et al., 2018; Shahsavari and Ameri, 2010).

The available energy of the BIPVT-SRHX system during the cooling mode is obtained as:

$$\dot{E}_{u,cooling} = \dot{E}_{u,TW-cooling} + \dot{E}_{u,BIPVT-cooling} \quad (19)$$

where

$$\dot{E}_{u,TW-cooling} = \dot{m}_f c_p (T_{h,i} - T_{h,o}) - \left(\frac{\dot{E}_{fan,c} + \dot{E}_{fan,h}}{0.36} \right) \quad (20)$$

$$\dot{E}_{u,BIPVT-cooling} = \frac{\dot{E}_{el,PV} - \dot{E}_{fan,BIPVT}}{0.36} \quad (21)$$

$$\dot{E}_{el,PV} = 0.13 \alpha_{pv} I_r WL [1 - 0.006(T_{pv} - 298)] \quad (22)$$

$$\dot{E}_{fan} = \frac{(\dot{m}_f / \rho) \Delta P}{\eta_{fan}} \quad (23)$$

In the above equation, η_{fan} denotes the fan efficiency and ΔP is the pressure loss which is computed for BIPVT and SRHX systems using the technique described in Shahsavari et al. (Shahsavari et al., 2018; Khanmohammadi and Shahsavari, 2018).

The available exergy of the BIPVT-SRHX system in the heating mode is computed as:

$$\dot{X}_{u,heating} = \dot{X}_{u,TW-heating} + \dot{X}_{u,BIPVT-heating} \quad (24)$$

where

$$\dot{X}_{u,TW-heating} = \dot{m}_f c_p \left[T_{c,o} - T_{c,i} - T_a \ln \left(\frac{T_{c,o}}{T_{c,i}} \right) \right] - \dot{X}_{fan,c} - \dot{X}_{fan,h} \quad (25)$$

$$\dot{X}_{u,BIPVT-heating} = \dot{m}_f c_p \left\{ T_f(L) - T_{c,o} - T_a \ln \left[\frac{T_f(L)}{T_{c,o}} \right] \right\} + \dot{X}_{el,PV} - \dot{X}_{fan,BIPVT} \quad (26)$$

The available exergy of the BIPVT-SRHX system in the cooling mode of operation is obtained as:

$$\dot{X}_{u,cooling} = \dot{X}_{u,TW-cooling} + \dot{X}_{u,BIPVT-cooling} \quad (27)$$

where

$$\dot{X}_{u,TW-cooling} = \dot{m}_f c_p \left[T_{h,i} - T_{h,o} - T_a \ln \left(\frac{T_{h,i}}{T_{h,o}} \right) \right] - \dot{X}_{fan,c} - \dot{X}_{fan,h} \quad (28)$$

$$\dot{X}_{u,BIPVT-cooling} = \dot{X}_{el,PV} - \dot{X}_{fan,BIPVT} \quad (29)$$

6. Exergo-economic analysis

Exergo-economic is an exergy based economic assessment which utilizes annual exergy with uniform end of annual cost for enhancing the performance of systems (Tsatsaronis and Morosuk, 2008). The goal of this assessment is to explore the cost-optimal structure, the cost optimal values and finally helps designers to obtain means for augmenting the performance of a system in a cost effective approach (Tsatsaronis and Morosuk, 2008). The exergo-economic aspect is defined as (Tiwari et al., 2015; Agrawal and Tiwari, 2012):

$$R_{ex} = \frac{\dot{X}_{dest,BIPVT} + \dot{X}_{dest,TW}}{P_s (1 + M_s) \left[\frac{i \times (1+i)^n}{(1+i)^n - 1} \right] - S_s \frac{i}{(1+i)^n - 1}} \quad (30)$$

where P_s is the net present cost, M_s is the maintenance cost (10%), i is the inflation rate, and S_s is the salvage value (5%) of the studied BIPVT-SRHX system.

Three DC fans, one in the BIPVT system and two in the SRHX, are utilized to flow the fresh and exhaust airs in the system. These fans should be replaced after 10 years. Therefore, the net present cost (P_s) for the 20 years life span of the studied PVT-SRHX system is:

$$P_s = P + P_f + \frac{P_f}{(1+i)^{10}} \quad (31)$$

where, P_f is the cost of fan and P is the initial cost of the system including the cost of PV modules (= 56.97WL), fans (702.2), SRHX (= 555.56D + 222.23), and inverter (= 33.57WL) (Shahsavari et al., 2018). It should be noted that the mentioned prices are in \$. These values are obtained by means of cost functions obtained from manufacturers data and/or rough estimations based on the assumptions of large-scale production.

7. Enviro-economic analysis

Enviro-economic assessment is the most powerful mechanism to boost the use of renewable energy technologies as it does not emit carbon (Tiwari et al., 2015). It is based on price of CO₂ emission and emitted carbon quantity. On average, a coal-based power plant produces 960 g CO₂ per kWh electricity (Sovacool, 2008). Considering the transmission and distribution losses, the amount of CO₂ per kWh comes to be 2.0 kg. Hence, CO₂ mitigation per year from to BIPVT-SRHX system is given as (Rajoria et al., 2013):

$$\varphi_{CO_2} = 0.002 (\dot{X}_{u,heating} + \dot{X}_{u,cooling}) \quad (32)$$

Now, the enviro-economic aspect or environmental cost is computed using the following equation (Tiwari et al., 2015):

$$R_{en} = z_{CO_2} \varphi_{CO_2} \quad (33)$$

where z_{CO_2} is the international carbon price (14.5 \$ per ton of CO₂ (Caliskan et al., 2012)).

8. Multi-objective genetic algorithm (MOGA) optimization

The performance parameters of some real-world systems are more than one, whose patterns of variation often conflict with each other. For example, in the case of PVT systems, thermal energy output, electrical energy output, and thermal exergy output can be considered as the performance parameters. Therefore, to optimize the performance of such systems, the designer must consider all the performance parameters simultaneously. The technique used for this purpose is multi-objective optimization (Hwang and Masud, 2012). In other words, one cannot find an ideal point where all the performance parameters at that point reach their optimal value. For these cases, there is a collection of optimal points determined by the concept of Pareto dominance. In MOGA, genetic algorithm is employed to obtain the Pareto based on the selection, mutation and crossover operations in the genetic algorithm. Therefore, optimal Pareto of MOGA is defined as an ideal vector that each individual components drives the objectives separately to their optimum solution.

This study presents a MOGA optimization with the annual exergo-economic (R_{ex}) and enviro-economic (R_{en}) objective functions. To find the optimum solution of the discussed BIPVT-SRHX system, seven independent aspects (geometrical and operating) were selected and listed with their constraint in Table 1. Fig. 4 represents a schematic diagram of the multi-objective procedure used in the current study.

9. Results and discussions

In this section, initially the developed mathematical model is validated, and then the exergo-economic and enviro-economic analyses of the BIPVT-SRHX system for Kermanshah, Iran climatic conditions are determined. For this purpose, first the energy and exergy performances of the system in various months of a year are examined. Then, the factors that influence the exergo-economic and enviro-economic aspects are determined and their influences are investigated. Finally, the multi-objective optimization is implemented to optimize the system performance from both exergo-economic and enviro-economic perspectives, and the performances of the optimized and non-optimized systems are compared. The climatic conditions of typical days of each individual month for Kermanshah are listed in Appendix A. In addition, the number of clear days per month in Kermanshah is presented in Table 2. It is noteworthy that the mass currents of the cold and hot air streams are similar.

9.1. Validation of the BIPVT model

In this work, the performance of the BIPVT-SRHX device is simulated using a MATLAB home-made code. For the validation of the numerical method, the numerical results of PV panel temperature and leaving air temperature are compared with the experimental outcomes of Tonui and Tripanagnostopoulos (<https://www.weather-atlas.com>). Fig. 5(a) and (b) respectively demonstrate the considered system and the findings of validation. The evaluated device is a classic PVT system equipped with

Table 1
Decision variables and their lower and upper boundaries.

Parameter	W (m)	L (m)	S (m)	\dot{m}_f (kg/s)	N (rpm)	l (m)	D (m)
Lower bound	0.5	1	0.1	0.569	0	0.2	0.5
Upper bound	5	10	0.5	5.69	20	1.5	2

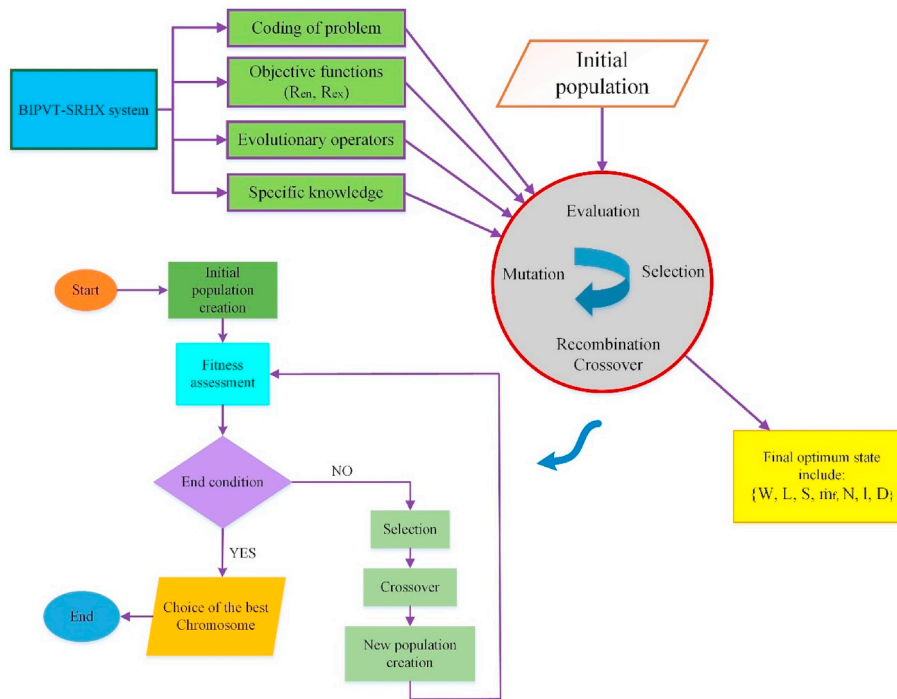


Fig. 4. Schematic diagram of multi-objective procedure used in the current study.

Table 2

Number of clear days per month in Kermanshah (<https://www.weather-atlas>).

Month	Jan.	Feb.	Mar.	Apr.	May.	Jun.	Jul.	Aug.	Sep.	Oct.	Nov.	Dec.
Number of clear days	20	18	19	19	24	30	31	31	30	27	23	22

an air channel located underneath the PV panel. Fig. 5(b) reveals that the employed mathematical model is significantly accurate.

9.2. System performance

The monthly available thermal, electrical and total energies of the BIPVT-SRHX system have been illustrated in Fig. 6. In the considered system $D = 1$ m, $l = 0.6$ m, $L = 5$ m, $\dot{m}_{f,c} = \dot{m}_{f,h} = \dot{m}_f = 1.0$ kg/s, $N = 10$ rpm, $S = 0.3$ m, $W = 1$ m. As observed, the thermal energy extracted from the device in various months of the year is higher than the electrical energy. According to the results, the annual sums of available thermal, electrical, and total energies of the studied system are 25414.1, 5837.9 and 41630.2 kWh, respectively.

Fig. 7 displays the monthly available thermal, electrical, and total exergies of the system. According to this figure, the share of electrical exergy in total exergy is much greater than the thermal exergy. Based on the results, the annual sums of available thermal, electrical, and total exergies obtained from the considered BIPVT-SRHX system are 298.7, 5837.9 and 6136.5 kWh, respectively.

The amount of CO₂ mitigation from the evaluated BIPVT-SRHX device in various months of a year have been illustrated in Fig. 8. According to Eq. (32), the amount of CO₂ mitigation from the proposed system is a function of available exergy and, therefore, its monthly variations resemble the variations of the available exergy of the system. The highest reduction in CO₂ emission is achieved in July (1.34 tons), while the lowest one occurs in November (0.63 tons). The findings show that utilizing the proposed system leads to prevention of 12.13 tons of CO₂ emission into the atmosphere, annually.

9.3. Case study of the BIPVT-SRHX system

Examining the used equations of the BIPVT-SRHX performance shows that the performance of this system is mainly affected by the following factors: the length, width and depth of the air duct below the PV modules, the mass current of fresh/exhaust air in heating/cooling modes, and the diameter, rotational velocity and length of the SRHX. The impacts of these aspects on the exergo-economic and enviro-economic aspects are investigated in this section.

Fig. 9 displays the impacts of air mass current on the exergo-economic and enviro-economic aspects of the system. As observed, the values of both of these aspects are reduced by increasing the air mass current. According to Eqs. (25), (26) and (28), boosting the air mass current results in an increase in the thermal exergy and thus the increase of available exergy of the system. Additionally, according to Eq. (23), the amount of electricity consumed by fans augments with intensifying the air mass current; which reduces the amount of available exergy of the system. Conversely, boosting the air mass current reduces the temperature of PV modules, thereby augments the amount of electricity produced by the modules and the available exergy of the system. Fig. 9 displays that the influence of intensification in the power consumed by fans overcomes the impact of increase in the thermal exergy and the electricity produced by PV modules, and the available exergy of the considered system declines by intensifying the air mass current. Since air mass current has no influence on the system cost, the reduction of available exergy of the device with the intensification of air mass current leads to the decrease of exergo-economic and enviro-economic aspects.

Fig. 10 shows the impacts of duct width on the exergo-economic and enviro-economic aspects of the system. As seen, increase in duct width, initially improves the exergo-economic aspect of the system then decreases after reaching a maximum value while the enviro-economic

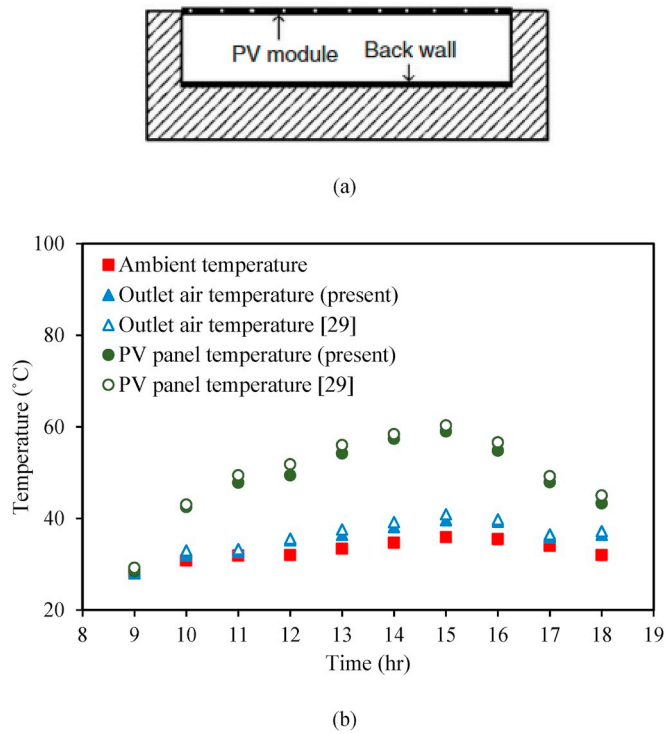


Fig. 5. (a) Schematic of the BIPVT system studied by Tonui and Tripanagnostopoulos (Tonui and Tripanagnostopoulos, 2006) and (b) comparison of experimental results (Tonui and Tripanagnostopoulos, 2006) and presented mathematical model.

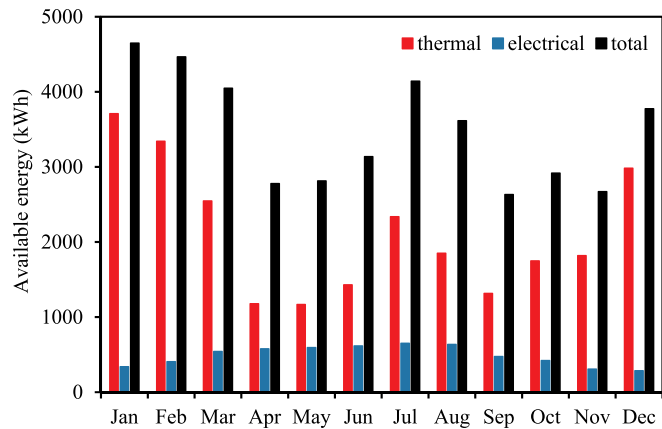


Fig. 6. The monthly available thermal, electrical and total energies of the BIPVT-SRHX system.

aspect almost linearly goes up. With constant air mass current, boosting the duct width causes a decrease in the air velocity and, thus, the rise in the temperature of exhaust air from the PV system, the reduction of consumed power by fans (due to the pressure loss reduction) and the reduction of generated electricity by PV modules (because of increase in the temperature of PV modules). Conversely, according to Eq. (22), intensifying the duct width directly rises the generated electricity by PV modules. The findings show that in general, the amount of electricity produced by PV modules improves with the increase of duct width. Considering the increased value of enviro-economic aspect with boosting the duct width in Fig. 9, it can be said that the impact of increase in the exhaust air temperature from the system and in the amount of generated electricity by modules overcomes the impact of increase in the amount of consumed power by fans, and the amount of available exergy

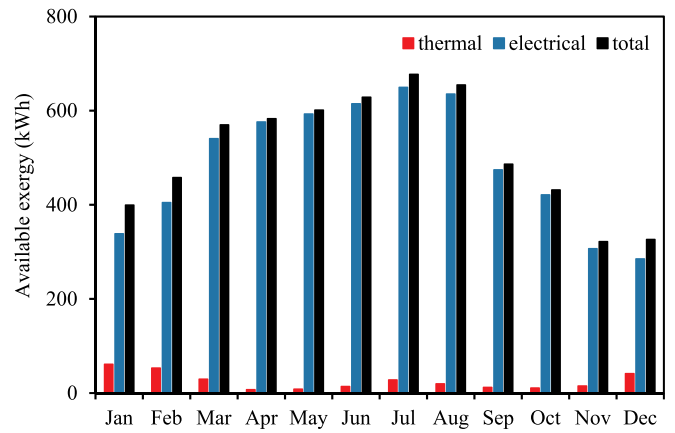


Fig. 7. The monthly available thermal, electrical and total exergies of the BIPVT-SRHX system.

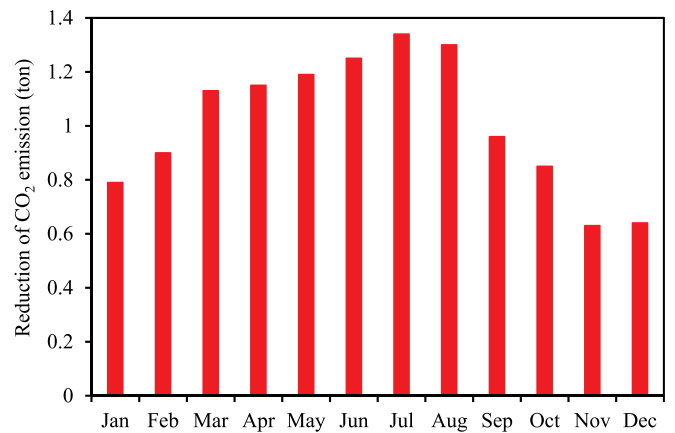


Fig. 8. The monthly amount of CO₂ mitigation from the BIPVT-SRHX system.

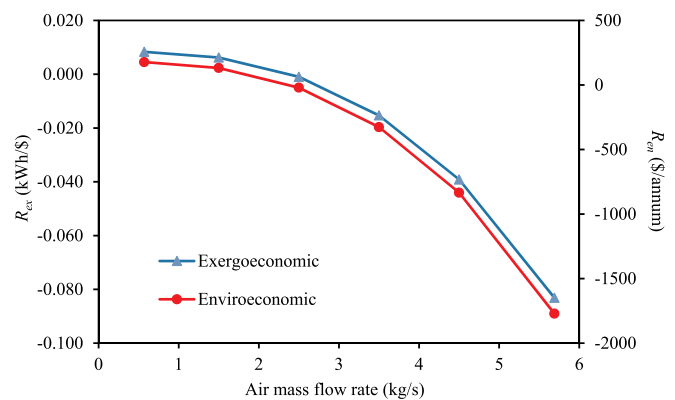


Fig. 9. Influence of air mass current on the exergo-economic and enviro-economic aspects.

of the system goes up with intensifying the duct width. Nevertheless, the increase of duct width leads to the increase of system cost and thus the reduction of exergo-economic aspect. Therefore, by looking at Fig. 10 it is realized that at small duct widths, the impact of increase of available exergy overcomes the impact of cost increase, and the value of exergo-economic aspect augments with the increase of duct width; while the opposite occurs with the further increase of duct width.

The influences of duct length on the exergo-economic and enviro-economic aspects of the system have been displayed in Fig. 11. As

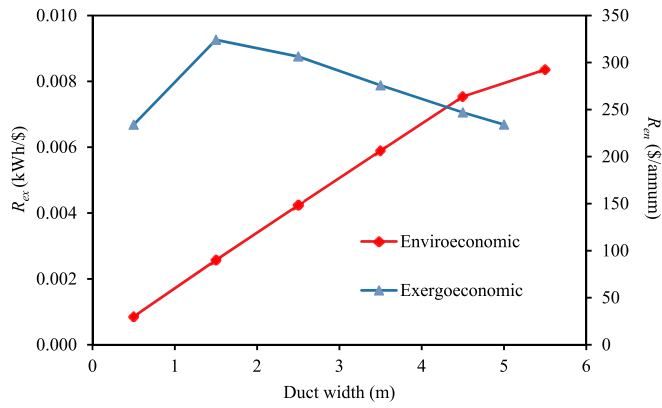


Fig. 10. Impact of duct width on the exergo-economic and enviro-economic aspects.

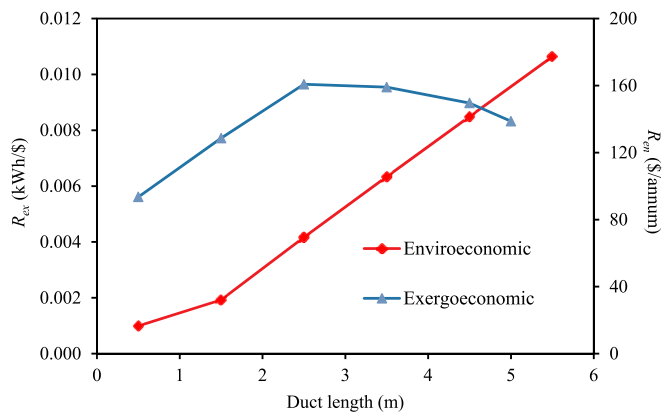


Fig. 11. Impact of duct length on the exergo-economic and enviro-economic aspects.

observed, with the increase of duct length, the value of enviro-economic aspect increases, while the exergo-economic aspect increases first and then decreases. The increase in duct length leads to the rise of exhaust air temperature, increase of the module generated electricity and also the increase of fan consumed power; which the first two factors increase the value of available exergy of the system and the third factor reduces the amount of available exergy. As shown in Fig. 11, the impact of increase in the temperature of exhaust air from the system and in the amount of electricity produced by PV panels outweighs the influence of increase in the amount of power consumed by fans, and the value of available exergy of system intensifies with augmenting the duct length; which increases the value of enviro-economic aspect. On the other hand, boosting the duct length results in an increase of system cost and thus the reduction of exergo-economic aspect. Fig. 11 shows that at small duct lengths, the impact of increase of available exergy overcomes the impact of cost increase, and the value of exergo-economic aspect rises with intensifying the duct length; while the opposite occurs with the further increase of duct length.

The influences of duct depth on the exergo-economic and enviro-economic aspects of the system have been demonstrated in Fig. 12. As displayed, the values of both aspects diminish with the increase of duct depth. Duo to the constant air mass current, augmenting the duct depth causes a decline in the air speed and, consequently, the rise in the temperature of exhaust air from the BIPVT collector, the reduction of power used by fans and the reduction of electricity produced by PV modules. Fig. 12 depicts that, as the duct depth augments, the impact of reduced electricity generation by PV modules overcomes the impact of exhaust air temperature rise and the impact of reduced power consumption by fans, and the amount of available exergy obtained from the

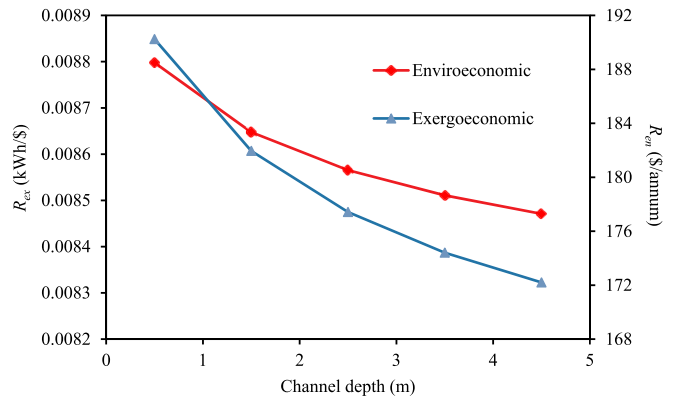


Fig. 12. Impact of duct depth on the exergo-economic and enviro-economic aspects.

system is diminished. Also, the greater drop in the value of exergo-economic aspect relative to enviro-economic aspect is due to the increase of system cost with the increase of duct depth.

Fig. 13 shows the impacts of the rotational velocity of SRHX on the exergo-economic and enviro-economic aspects of the system. As seen, with augmenting the rotational velocity of the SRHX, the values of both aspects increase slightly at first and then remain almost constant. Boosting the rotational speed of SRHX leads to the increase of effectiveness and, as a result, the increase of heat exchange between cold and warm airs, which eventually results in the augmentation of available exergy of the considered system. On the other hand, as the rotational speed of the SRHX increases, it consumes more electrical power and, as a result, the available exergy of the system diminishes. Based on the results presented in Fig. 13, at low rotational speeds, the impact of increased heat transfer is greater than the impact of increased power consumption by the SRHX and, therefore, the amount of available exergy of the system and the values of both the exergo-economic and enviro-economic aspects increase; however at higher rotational speeds, the two discussed impacts are almost equal in strength and the values of both aspects also remain almost constant.

Fig. 14 illustrates the impacts of SRHX length on the exergo-economic and enviro-economic aspects of the system. The results indicate that both of these aspects diminish with the increase of SRHX length. Intensifying the SRHX length, on the one hand, leads to the increase of heat transfer surface area and thus, the increase of available exergy of the unit and, on the other hand, it boosts the pressure drop and, consequently, the fan power; which reduces the amount of available exergy of the system. Fig. 14 demonstrates that the impact of the augmented fan power overcomes the impact of heat transfer increase, and the amount of available exergy of the system and therefore, the values of the exergo-economic and enviro-economic aspects diminish

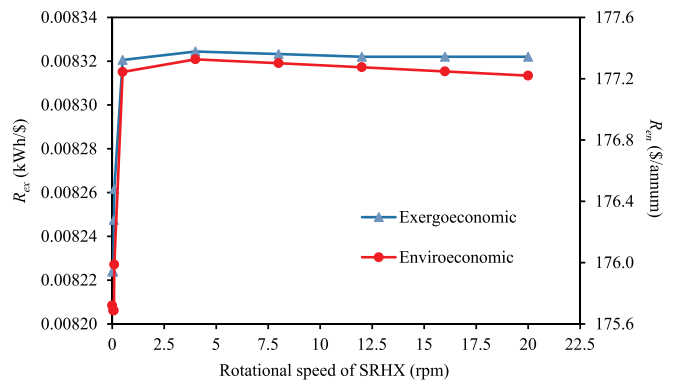


Fig. 13. Impact of the rotational speed of SRHX on the exergo-economic and enviro-economic aspects.

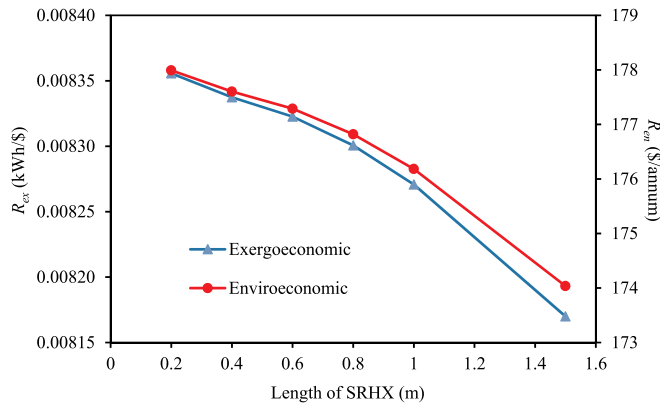


Fig. 14. Impact of SRHX length on the exergo-economic and enviro-economic aspects.

with the increase of SRHX length.

Fig. 15 displays the impacts of SRHX diameter on exergo-economic and enviro-economic aspects of the system. The findings depict that boosting the SRHX diameter reduces the exergo-economic aspect and increases the enviro-economic aspect. The increase of SRHX diameter reduces the air speed and, therefore, the pressure losses of cold and hot air flows inside the SRHX, and thereby reduces the power needed by the cold and hot air fans. On the other hand, the temperature of fresh air coming out of the SRHX boosts in the winter and drops in the summer by reducing the air flow velocity. Both of these occurrences boost the available exergy of the system and, consequently, increases the exergo-economic and enviro-economic aspects of the system. In addition, the increase of SRHX diameter adds to system cost and, thus, reduces the exergo-economic aspect. The results presented in Fig. 15 show that the influence of system cost increase overcomes the influence of the increase of available exergy of the system, and the exergo-economic aspect diminishes with the increase of SRHX diameter.

9.4. Optimization of the BIPVT-SRHX system

In this section, the optimization findings of the studied system are discussed. By using multi-objective optimization and employing an evolutionary GA, the optimum values for the defined objective functions (i.e., exergo-economic and enviro-economic aspects) have been determined in the form of Pareto diagrams. In the studied problem, both objective functions are maximized.

Fig. 16 shows the two-objective optimization results as Pareto front. The illustrated points indicate the non-dominant solutions for the optimization problem based on the defined objective functions. Considering

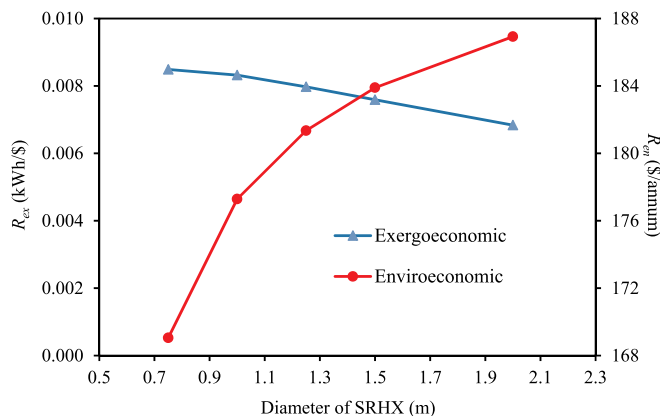


Fig. 15. Impact of wheel diameter on the exergo-economic and enviro-economic aspects.

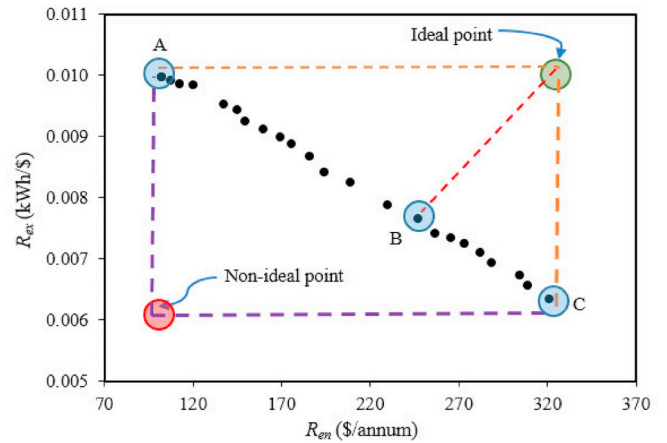


Fig. 16. Pareto front diagram for the exergo-economic and enviro-economic aspects.

the nature of two-objective optimization, all the presented points in the figure constitute the solutions of the optimization problem, and choosing a specific point for design depends on the discretion of designers. In this regard, various criteria can be used to select an optimal point. Here, ideal and non-ideal points are used in choosing a desired point. By definition, an ideal point is the point at which both defined objective functions are in their best possible state. Conversely, a non-ideal point corresponds to the worst possible state for the objective functions. One criterion for choosing an optimal point is to select a point with the least geometrical distance from the ideal point on the Pareto graph. By considering this criterion, point B is regarded as a desired point with an optimal state.

The specifications of the points shown on the Pareto front, including points A, B and C, have been listed in Table 3. Points A and C correspond to the optimal points in single-objective optimization in which the exergo-economic aspect and the enviro-economic aspect is considered as the objective function, respectively.

Sensitivity analyses of the objectives, reveals that the most sensitive aspects of this optimization are rotational speed of the SRHX, duct depth and mass current of the air while the optimization is less sensitive to the other aspects (please see Fig. 17). According to sensitivity analysis, the utopian range of the most sensitive independent aspects are the narrowest and since the variations are so small, these range can be approximated with almost a single value (rotational speed of the SRHX: 1.21 rpm, duct depth: 0.15 m and mass current of the air: 5.69 kg/s) while the rest of independent aspects have wider utopian ranges (duct width: 2.5–5 m, duct length: 2–10 m, length of SRHX: 0.5–0.9 m and diameter of SRHX: 1–1.2 m).

Hereafter, the BIPVT-SRHX system with characteristics of point B is named the optimized system and the system examined in section 9.2 is named non-optimized system. Fig. 18 shows the enviro-economic aspect of the optimized and the non-optimized BIPVT-SRHX systems in various months. It is observed that the values of enviro-economic aspect are improved through the optimization. Both the optimized and non-optimized units have their highest and lowest enviro-economic aspect in July and November, respectively. The yearly average enviro-economic aspect of the optimized and the non-optimized systems is 242.58 and 177.29, respectively.

The reductions of carbon dioxide emission by the optimal and the non-optimal systems throughout a year have been displayed in Fig. 19. As displayed, throughout a year, more CO₂ is reduced by the optimized system than the non-optimized system. The yearly sum of CO₂ mitigation of the optimized and the non-optimized systems are 16.73 and 12.15 ton, respectively.

Fig. 20 illustrates the monthly variations of the exergo-economic aspect of the optimized and the non-optimized systems. Throughout a

Table 3

The optimum decision variables and the values of objective functions for selected points on the Pareto front diagram.

Points	Objective functions		Decision variables						
	R_{en} (\$/annum)	R_{ex} (kWh/\$)	w(m)	L(m)	s(m)	\dot{m}_f (kg/s)	N(rpm)	l(m)	D (m)
A	102.32	0.0100	2.79	5.98	0.15	0.63	1.09	0.77	1.02
B	246.94	0.0076	4.19	9.52	0.14	0.76	1.21	0.56	1.15
C	321.31	0.0063	4.99	9.99	0.17	1.31	1.48	0.88	1.84

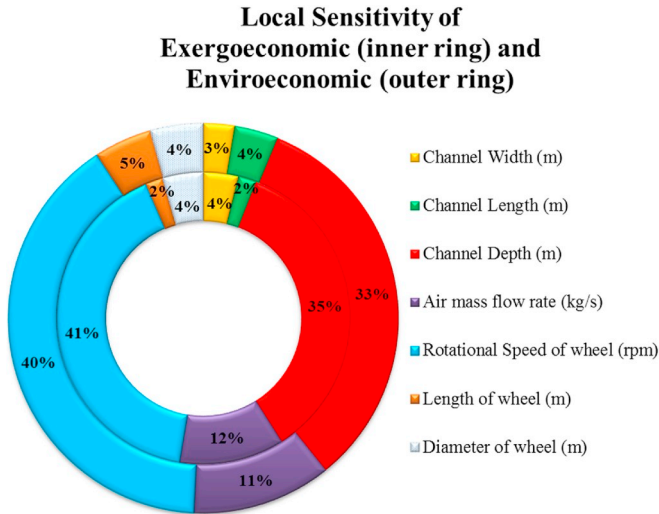


Fig. 17. Local sensitivity of exergo-economic and enviro-economic vs. independent aspects.

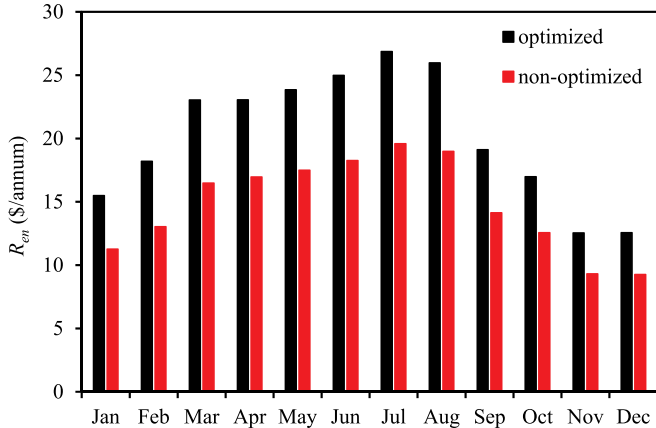


Fig. 18. Enviro-economic aspect of the optimized and non-optimized BIPVT-SRHX systems in various months.

year, the exergo-economic of the non-optimized system is greater than the optimized system. The annual average exergo-economic aspect of the optimized system is 23.1% greater compare with the non-optimized system.

10. Conclusion

This numerical investigation proposes a novel hybrid BIPVT-SRHX system that uses the exhaust air to intensify/decline the outdoor air temperature in winter/summer and to enhance the amount of electricity produced by the PV modules. The performance of the system is analyzed and optimized from exergo-economic and enviro-economic perspectives. The highlighted conclusions are drawn below:

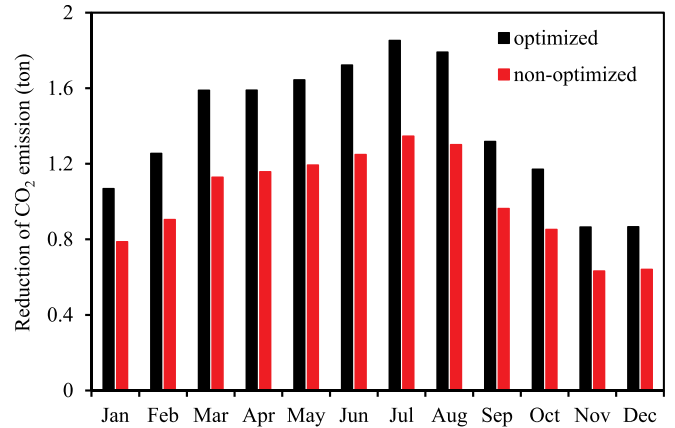


Fig. 19. Reduced CO₂ emission from the optimized and non-optimized BIPVT-SRHX systems in various months.

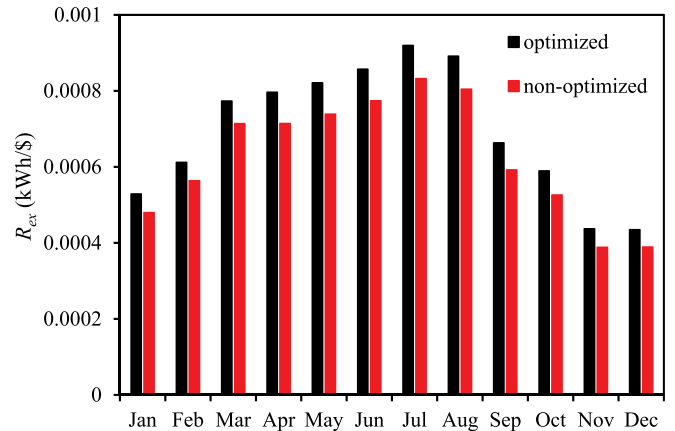


Fig. 20. Monthly variations of the exergo-economic aspect of the optimized and non-optimized BIPVT-SRHX systems.

- The yearly sum of available energy and exergy of the non-optimized BIPVT-SRHX system are 41630.2 and 6136.5 kWh whereas the yearly sum of CO₂ mitigation by this system is 12.13 ton.
- The exergo-economic aspect reduces by augmenting duct depth, flow rate, SRHX length, and SRHX diameter. In addition, the exergo-economic aspect first rises and then reduces with intensifying the duct length, duct width, and rotational speed of SRHX.
- The enviro-economic aspect increases with augmenting duct width, duct length, and SRHX diameter, while it reduces by increasing duct depth, flow rate, and SRHX length. Additionally, the enviro-economic aspect first increases and then decreases with the increase of rotational speed of SRHX.
- The optimum amounts of the design aspects for the considered BIPVT-SRHX system are $L = 9.52\text{ m}$, $W = 4.19\text{ m}$, $S = 0.14\text{ m}$, $\dot{m}_f = 0.76\text{ kg/s}$, $l = 0.56\text{ m}$, $D = 1.15\text{ m}$, and $N = 1.21\text{ rpm}$.

- The annual average exergo-economic and enviro-economic aspects of the optimized BIPVT-SRHX system are 0.0076 \$/annum and 246.94 kWh/\$, respectively.
- Optimization leads to a 36.8%, 23.1% and 37.7% increase in the annual average enviro-economic aspect, annual average exergo-economic aspect, and yearly sum of CO₂ mitigation of the BIPVT-SRHX system, respectively.

Declaration of interest

None

Acknowledgments

This research is supported by the Education Integration project of Ministry of Education (201801192032).

Appendix A. Considered weather conditions for Kermanshah

Hour	January		February		March		April	
	$I_r(W/m^2)$	$T_a(K)$	$I_r(W/m^2)$	$T_a(K)$	$I_r(W/m^2)$	$T_a(K)$	$I_r(W/m^2)$	$T_a(K)$
00	0	277.75	0	279.05	0	284.55	0	289.45
01	0	277.05	0	278.35	0	283.75	0	288.65
02	0	276.45	0	277.75	0	283.15	0	288.05
03	0	275.95	0	277.25	0	282.75	0	287.65
04	0	275.85	0	277.15	0	282.55	0	287.45
05	0	276.15	0	277.45	0	282.85	69.2	287.75
06	0	276.85	32	278.15	165	283.65	292.4	288.55
07	141.2	278.25	249.5	279.55	395.6	284.95	506.2	289.85
08	333.8	280.15	454	281.45	596.6	286.95	688.4	291.85
09	486	282.45	614.4	283.75	751.2	289.15	826.2	294.05
10	583.4	284.95	718.3	286.35	848.3	291.75	910.3	296.65
11	618.7	287.35	758.2	288.75	881	294.15	935	299.05
12	589.4	289.15	731.2	290.55	847	295.95	898.7	300.85
13	497.6	290.35	639.2	291.75	748.9	297.15	803.8	302.05
14	350.1	290.85	488.9	292.15	593.3	297.55	656.8	302.45
15	160.2	290.35	291.6	291.75	391.5	297.15	467.5	302.05
16	0	289.35	70.2	290.65	160.7	296.05	249.5	300.95
17	0	287.65	0	289.05	0	294.45	32.9	299.35
18	0	285.75	0	287.05	0	292.45	0	297.35
19	0	283.75	0	285.15	0	290.55	0	295.45
20	0	282.15	0	283.45	0	288.85	0	293.75
21	0	280.65	0	281.95	0	287.35	0	292.25
22	0	279.45	0	280.75	0	286.15	0	291.05
23	0	278.55	0	279.85	0	285.25	0	290.15
Hour	May		June		July		August	
	$I_r(W/m^2)$	$T_a(K)$	$I_r(W/m^2)$	$T_a(K)$	$I_r(W/m^2)$	$T_a(K)$	$I_r(W/m^2)$	$T_a(K)$
00	0	294.35	0	297.35	0	300.55	0	298.95
01	0	293.55	0	296.55	0	299.95	0	298.25
02	0	292.95	0	295.95	0	299.45	0	297.65
03	0	292.55	0	295.55	0	298.85	0	297.15
04	0	292.35	0.3	295.35	3.4	298.65	0	297.05
05	81.7	292.65	168.7	295.65	180.9	299.35	136	297.35
06	309.5	293.45	388.3	296.45	394.6	299.65	353.3	298.05
07	526.2	294.75	591.2	297.75	592.6	301.55	556.6	299.45
08	710.1	296.75	762.1	299.75	769.5	303.45	730.2	301.35
09	848	298.95	889.3	301.95	899.6	305.45	862.6	303.65
10	930.5	301.55	964.3	304.55	967.7	308.25	944.7	306.15
11	951.8	303.95	981.9	306.95	985.5	310.75	971.2	308.55
12	910.5	305.75	941.1	308.75	950.8	312.65	940.3	310.35
13	809.5	306.95	844.6	309.95	862.1	314.05	854	311.55
14	658.7	307.35	698.8	310.35	725.2	314.25	718.1	312.05
15	479.7	306.95	513.6	309.95	549.3	313.35	541.7	311.55
16	256.1	305.85	301.9	308.85	346.2	312.65	336.6	310.55
17	44.9	304.25	83.4	307.25	132	311.05	119.4	308.85
18	0	302.25	0	305.25	0	308.85	0	306.95
19	0	300.35	0	303.35	0	306.95	0	304.95
20	0	298.65	0	301.65	0	305.55	0	303.35
21	0	297.15	0	300.15	0	303.85	0	301.85
22	0	295.95	0	298.95	0	302.65	0	300.65
23	0	295.05	0	298.05	0	301.95	0	299.75
Hour	September		October		November		December	
	$I_r(W/m^2)$	$T_a(K)$	$I_r(W/m^2)$	$T_a(K)$	$I_r(W/m^2)$	$T_a(K)$	$I_r(W/m^2)$	$T_a(K)$
00	0	296.55	0	291.45	0	286.75	0	280.55
01	0	295.75	0	290.65	0	286.05	0	279.75
02	0	295.15	0	290.05	0	285.45	0	279.15
03	0	294.75	0	289.65	0	284.95	0	278.75
04	0	294.55	0	289.45	0	284.85	0	278.55

(continued on next page)

(continued)

Hour	January		February		March		April	
	$I_r(W/m^2)$	$T_a(K)$	$I_r(W/m^2)$	$T_a(K)$	$I_r(W/m^2)$	$T_a(K)$	$I_r(W/m^2)$	$T_a(K)$
05	8.5	294.85	0	289.75	0	285.15	0	278.85
06	216.3	295.65	134.4	290.55	27.3	285.85	0	279.65
07	435.8	296.95	349.4	291.85	221.7	287.25	134.4	280.95
08	621	298.95	530.8	293.85	399.2	289.15	314.3	282.95
09	757.6	301.15	661.9	296.05	529.4	291.45	452.6	285.15
10	836	303.75	733.1	298.65	601.7	293.95	535.8	287.75
11	850.8	306.15	739.4	301.05	610.7	296.35	557.5	290.15
12	801.1	307.95	680.2	302.85	555.7	298.15	516.1	291.95
13	690.1	309.15	559.9	304.05	440.8	299.35	414.6	293.15
14	525.7	309.55	387.1	304.45	275	299.85	261.3	293.55
15	319.7	309.15	176.5	304.05	77.6	299.35	74.6	293.15
16	92.4	308.05	0.1	302.95	0	298.35	0	292.05
17	0	306.45	0	301.35	0	296.65	0	290.45
18	0	304.45	0	299.35	0	294.75	0	288.45
19	0	302.55	0	297.45	0	292.75	0	286.55
20	0	300.85	0	295.75	0	291.15	0	284.85
21	0	299.35	0	294.25	0	289.65	0	283.35
22	0	298.15	0	293.05	0	288.45	0	282.15
23	0	297.25	0	292.15	0	287.55	0	281.25

References

- Agrawal, S., Tiwari, G., 2012. Exergoeconomic analysis of glazed hybrid photovoltaic thermal module air collector. *Sol. Energy* 86, 2826–2838.
- Calise, F., Figaj, R.D., Massarotti, N., Mauro, A., Vanoli, L., 2017. Polygeneration system based on PEMFC, CPVT and electrolyzer: dynamic simulation and energetic and economic analysis. *Appl. Energy* 192, 530–542.
- Caliskan, H., Dincer, I., Hepbasli, A., 2012. Exergoeconomic, enviroeconomic and sustainability analyses of a novel air cooler. *Energy Build.* 55, 747–756.
- Chen, H., Zhang, L., Jie, P., Xiong, Y., Xu, P., Zhai, H., 2017. Performance study of heat-pipe solar photovoltaic/thermal heat pump system. *Appl. Energy* 190, 960–980.
- Di Capua, M., Escobar, R., Diaz, A.J., Guzman, A.M., 2018. Enhancement of the cooling capability of a high concentration photovoltaic system using microchannels with forward triangular ribs on sidewalls. *Appl. Energy* 226, 160–180. <https://www.weather-atlas.com/en/iran/kermanshah-climate>.
- Hwang, C.L., Masud, A.S.M., 2012. Multiple Objective Decision Making Methods and Applications: a State-Of-The-Art Survey. Springer Science & Business Media.
- Khaki, M., Shahsavari, A., Khanmohammadi, S., Salmazadeh, M., 2017. Energy and exergy analysis and multi-objective optimization of an air based building integrated photovoltaic/thermal (BIPV/T) system. *Sol. Energy* 158, 380–395.
- Khaki, M., Shahsavari, A., Khanmohammadi, S., 2018. Scenario-based multi-objective optimization of an air-based building-integrated photovoltaic/thermal system. *J. Sol. Energy Eng.* 140, 011003.
- Khanmohammadi, S., Shahsavari, A., 2018. Energy analysis and multi-objective optimization of a novel exhaust air heat recovery system consisting of an air-based building integrated photovoltaic/thermal system and a thermal wheel. *Energy Convers. Manag.* 172, 595–610.
- Liu, Z., Zhang, Y., Zhang, L., Luo, Y., Wu, Z., Wu, J., Yin, Y., Hou, G., 2018. Modeling and simulation of a photovoltaic thermal-compound thermoelectric ventilator system. *Appl. Energy* 228, 1887–1900.
- Modjinou, M., Ji, J., Li, J., Yuan, W., Zhou, F., 2017. A numerical and experimental study of micro-channel heat pipe solar photovoltaics thermal system. *Appl. Energy* 206, 708–722.
- Mousavi, S., Kasaiean, A., Shafii, M.B., Jahangir, M.H., 2018. Numerical investigation of the effects of a copper foam filled with phase change materials in a water-cooled photovoltaic/thermal system. *Energy Convers. Manag.* 163, 187–195.
- Nahar, A., Hasanuzzaman, M., Rahim, N.A., Parvin, S., 2019. Numerical investigation on the effect of different parameters in enhancing heat transfer performance of photovoltaic thermal systems. *Renew. Energy* 132, 284–295.
- Rajoria, C., Agrawal, S., Tiwari, G., 2013. Exergetic and enviroeconomic analysis of novel hybrid PVT array. *Sol. Energy* 88, 110–119.
- Shahsavari, A., Ameri, M., 2010. Experimental investigation and modeling of a direct-coupled PV/T air collector. *Sol. Energy* 84, 1938–1958.
- Shahsavari, A., Khanmohammadi, S., 2019. Feasibility of a hybrid BIPV/T and thermal wheel system for exhaust air heat recovery: energy and exergy assessment and multi-objective optimization. *Appl. Therm. Eng.* 146, 104–122.
- Shahsavari, A., Rajabi, Y., 2018. Exergoeconomic and enviroeconomic study of an air based building integrated photovoltaic/thermal (BIPV/T) system. *Energy* 144, 877–886.
- Shahsavari, A., Salmazadeh, M., Ameri, M., Talebizadeh, P., 2011. Energy saving in buildings by using the exhaust and ventilation air for cooling of photovoltaic panels. *Energy Build.* 43, 2219–2226.
- Shahsavari, A., Khanmohammadi, S., Khaki, M., Salmazadeh, M., 2018. Performance assessment of an innovative exhaust air energy recovery system based on the PV/T-assisted thermal wheel. *Energy* 162, 682–696.
- Sharaf, O.Z., Orhan, M.F., 2018. Comparative thermodynamic analysis of densely-packed concentrated photovoltaic thermal (CPVT) solar collectors in thermally in-series and in-parallel receiver configurations. *Renew. Energy* 126, 296–321.
- Singh, D.B., Tiwari, G.N., 2017. Exergoeconomic, enviroeconomic and productivity analyses of basin type solar stills by incorporating N identical PVT compound parabolic concentrator collectors: a comparative study. *Energy Convers. Manag.* 135, 129–147.
- Sovacool, B.K., 2008. Valuing the greenhouse gas emissions from nuclear power: a critical survey. *Energy Policy* 36, 2940–2953.
- Tiwari, G., Yadav, J., Singh, D., Al-Helal, I., Abdel-Ghany, A.M., 2015. Exergoeconomic and enviroeconomic analyses of partially covered photovoltaic flat plate collector active solar distillation system. *Desalination* 367, 186–196.
- Tonui, J.K., Tripanagnostopoulos, Y., 2006. Improved PV/T solar collectors with heat extraction by forced or natural air circulation. *Sol. Energy* 81, 498–511.
- Tripathi, R., Tiwari, G.N., Dwivedi, V.K., 2017. Energy matrices evaluation and exergoeconomic analysis of series connected N partially covered (glass to glass PV module) concentrated-photovoltaic thermal collector: at constant flow rate mode. *Energy Convers. Manag.* 145, 353–370.
- Tsatsaronis, G., Morosuk, T., 2008. A general exergy-based method for combining a cost analysis with an environmental impact analysis. Part I-theoretical development. In: ASME 2008 International Mechanical Engineering Congress and Exposition. Boston, Massachusetts, USA, October 31–November 6.
- Xia, L., Ma, Z., Kokogiannakis, G., Wang, S., Gong, X., 2018. A model-based optimal control strategy for ground source heat pump systems with integrated solar photovoltaic thermal collectors. *Appl. Energy* 228, 1399–1412.
- Yu, B., Jiang, Q., He, W., Liu, S., Zhou, F., Ji, J., Xu, G., Chen, H., 2018. Performance study on a novel hybrid solar gradient utilization system for combined photocatalytic oxidation technology and photovoltaic/thermal technology. *Appl. Energy* 215, 699–716.